Check for updates

OPEN

The Southern Ocean with the largest uptake of anthropogenic nitrogen into the ocean interior

Xianliang L. Pan[1] ✉, Bofeng F. Li[2] & Yutaka W. Watanabe[2]

The oceanic external nitrogen (N_{ex}) deposition to the global ocean is expected to rise significantly owing to human activities. The Southern Ocean (SO) is an important pathway, which brings external influences into the ocean interior. It touches the borders of several developing countries that emit a large amount of anthropogenic nitrogen. To comprehend the dynamics of N_{ex} in the SO, we developed a new method to assess the change in the oceanic uptake of N_{ex} (ΔN_{ex}) in the entire SO. We obtained the spatiotemporal distribution of ΔN_{ex} in the SO by applying this method to a high-resolution grid data constructed using ship-based observations. During the 1990s to the 2010s, N_{ex} increased significantly by 67 ± 1 Tg-N year^{-1} in the SO. By comparing this value with the rate of N_{ex} deposition to the ocean, the SO has received ~70% of N_{ex} deposition to the global ocean, indicating that it is the largest uptake region of anthropogenic nitrogen into the ocean interior.

The reactive nitrogen (N_r, i.e. NO_x, NH_y, and dissolved organic nitrogen) input to the open ocean has increased significantly since 1860, especially in the last two decades[1]. Such consistent increase in the reactive nitrogen input could lead to changes in the ocean nitrogen and carbon cycles apart from affecting the marine biological productivity. Anthropogenic nitrogen released by human activities such as industrial nitrogen fixation and combustion of fossil fuel has contributed the most towards this increase. Nearly 70% of oceanic external nitrogen (N_{ex}), which is defined as the input of fluvial and atmospheric N_r in this study, is anthropogenic N_r[2]. Considering that the turnover time of natural N_r in the ocean is approximately 3,000 years[3,4], the change in N_{ex} (ΔN_{ex}) on the decadal timescale can closely reflect the change in the anthropogenic uptake in the ocean. The distribution of ΔN_{ex} in the surface ocean has been reported by several studies[1,5,6]. However, the spatiotemporal distribution of ΔN_{ex} in the ocean interior is yet to be revealed clearly; consequently, we lack the comprehension of the amount and storage of anthropogenic nitrogen received by the ocean as well as the variation in the oceanic uptake of anthropogenic nitrogen with time.

The Southern Ocean (SO, south of 30°S) covers approximately 30% of the global ocean surface area, and it is an important pathway that drives external influences such as anthropogenic impact into the global ocean interior owing to the strong movement of water masses (e.g. meridional overturning circulation)[7]. The SO is also very susceptible to anthropogenic materials because much of the sea surface water flowing into the SO touches the borders of several developing countries such as China, India, and South-East Asian countries. Therefore, clarifying the ocean dynamics of N_{ex} in the SO is crucial for gaining a deep understanding of the human impact on the ocean.

However, there are two challenges in exploring the presence of N_{ex} in the SO. One is the difficulty in acquiring ocean observations owing to the severe environmental condition of the SO. Ship-based observational data of the SO are considerably deficient compared with those of other oceans in the Northern Hemisphere. Recent studies on climate change in the SO have mainly focused on multiple repeated ship-based observations along the same lines every decade; the data collected is sparse owing to the difficulty in collecting data from the entire SO[8,9]. The other challenge is difficulty in separating N_{ex} from the internal nitrogen (recycled nitrogen, N_{in}). Kim *et al.* (2014) reported the impact of anthropogenic nitrogen on the western North Pacific using N^* and the water mass age[6]. Their approach could not remove the effect of nitrogen fixation and denitrification; consequently, it was difficult to estimate the anthropogenic nitrogen in the ocean accurately and apply it to the global ocean.

Recently, a new method capable of estimating the change in anthropogenic CO_2 impact on the ocean interior across decadal time intervals using parameterization techniques was proposed[10], which makes it possible to

[1]Graduate School of Environmental Science, Hokkaido University, Sapporo, Japan. [2]Faculty of Environmental Earth Science, Hokkaido University, Sapporo, Japan. ✉e-mail: panxianliang@ees.hokudai.ac.jp

1

overcome the two abovementioned difficulties related to the SO. Here, we have extended this method to N_{ex} and attempted to obtain the spatiotemporal distribution of ΔN_{ex} in the entire SO.

Results and Discussion

Parameterization of reactive nitrogen. We use nitrate (N) to represent N_r because nitrate accounts for more than 90% of N_r and it is the most stable dissolved form of nitrogen in the interior ocean (where most of ammonium and organic nitrogen are already conversed into N through nitrification or remineralization)[3]. The parameterization technique allows us to reconstruct the nitrate concentration spatiotemporally in the SO by using other hydrographic properties[11]. We used the hydrographic data for dissolved oxygen (DO or O_2), water temperature (T), salinity (S), and pressure (Pr) along with the observed N (N_{obs}) to perform the parameterization of N in the SO. All the data we used were sourced from Global Ocean Data Analysis Project version 2 (GLODAP v2), Climate and Ocean: Variability, Predictability and Change (CLIVAR), and Carbon Hydrographic Data Office (CCHDO) (https://cchdo.ucsd.edu/; Table S1 and Fig. S1(a))[12,13]. By giving several data constraints in obtaining an optimal parameterization (Table S2), we obtained the predicted concentration of N (N_p) in the SO, as follows:

$$N_p = 394.3 - 9.208 \times 10^{-2} \cdot DO - 1.534 \cdot T - 9.862 \cdot S + 2.029 \times 10^{-4} \cdot Pr \tag{1}$$

(Number of data points (n) = 65,257; Coefficient of determination (R^2) = 0.97; Root-mean-square error (RMSE) = 0.80 μmol kg^{-1})

More details of our parameterization method are presented in Figs. S2 and S3 and Table S3. Several statistical tests and an independent dataset were used to confirm the accuracy of our parameterization method (see Supplementary Text S2 for details). Additionally, we compared the spatial distributions of N_{obs} and N_p in the SO of 30°S south at surface, 500 m, 1,500 m, 3,000 m and 5,000 m (Fig. S4); consequently, the distribution of N_p was in good agreement with that of N_{obs}, demonstrating that our parameterization has high accuracy and applicability to the reconstruction of N in the entire SO.

Oceanic uptake of external nitrogen

Separation of N_{ex} from oceanic N. N_{obs} comprises an internal term (N_{in}) and an external term (N_{ex}) because the modern hydrographic data we used were already influenced by changes in the external matter. Heretofore, the separation of these two terms of N_{obs} was challenging. A method to estimate the variation in the external term of the observed ocean carbon species across different arbitrary years was proposed recently[10]. This method could be extended to distinguish N_{in} and N_{ex} (see Supplementary Text S4). We assumed that N_{ex} contained in N_p is the average N_{ex} between 2000 and 2016 ($N_{ex\,2008}$) and it remains constant with time due to the use of cruise data from 2000 to 2016 for constructing the parameterization of N_p. We can estimate the variation in N_{in} by considering the difference in N_p across different years (ΔN_p) due to the difference in N_{ex} as zero. The variation in N_{ex} (ΔN_{ex}) can be obtained by subtracting ΔN_p from the variation in the observed N (ΔN_{obs}) (Fig. S6; Eqs. (S2–S5)). Here, N_{in} includes the nitrate originating from the processes associated with DO, T, S, and Pr in the ocean, such as biological nitrogen fixation and remineralization; N_{ex} represents only the effects of atmospheric deposition and riverine nitrogen.

Through this method, we noticed that we could estimate ΔN_{ex} for a particular place by using ΔN_p along with the data for ΔN_{obs} of that place for different years (Fig. S6(b)). In order to draw the cross sections of ΔN_{ex} in the SO, we selected three repeated observations from the 1990s to the 2010s along the lines SR03, I08, and A12 as the representative data for the Pacific, Indian, and Atlantic basins (Fig. S7). Considering the uncertainty of the N_p parameterization (RMSE = 0.80 μmol kg^{-1}) and the propagation of uncertainty from the calculation (Eq. (S5)), ΔN_{ex} has an uncertainty of 1.13 μmol kg^{-1}, which means that ΔN_{ex} larger than this value must be significant. We estimated the meridional distributions of total water column inventory of ΔN_{ex} along each section (Fig. 1) by integrating ΔN_{ex} from the surface to the sea floor. Both SR03 and A12 have high water column inventories of ΔN_{ex} between the Antarctic Polar Front and the Subantarctic Front (50°S to 55°S), and both I08 and A12 near the Antarctic continent (60°S) also show high water column inventories of ΔN_{ex}. Considering the low primary production on the surface of the SO[14], the N_{ex} deposited on the surface must mainly enter the ocean interior through the formation of intermediate and deep waters and the penetration of surface water mass in the SO[15]. The Antarctic Circumpolar Current has become more active due to the strengthening of the westerly winds caused by the Southern Annular Mode, which has been increasing in the past two decades[16]. This phenomenon has strengthened the vertical exchanges of water masses in the SO, which supports the inference that there were remarkable increases in N_{ex} during the past 20 years in the Antarctic Intermediate Water and the Antarctic Bottom Water (Fig. S7).

Spatiotemporal distributions of ΔN_p and ΔN_{ex} over the Southern Ocean. Here, we used the same method as the previous sub-section to understand the distributions of ΔN_p (variation in internal N) and ΔN_{ex} over the entire SO. Considering the lack of observational data in the SO and the necessity for repeated observational data for the same location, we selected the observational data corresponding to the period 1990–1999 to represent the 1990s, 2000–2009 to represent the 2000s, and 2010–2017 to represent the 2010s. The data of each period were interpolated onto a common grid (see Supplementary Text S3). We used a grid with horizontal resolution of 1° × 1°, and 43 vertical layers with 50-m thickness from the surface to 500 m, 100-m thickness from 600 m to 1,500 m, and 200-m thickness from 1,700 m to the sea floor.

Seasonal differences between different cruises may affect our estimation. Owing to the severe environment of the SO, most of our observed data were collected in the warm period. In order to verify whether there was a significant difference between the data for cold period (for convenience, we call it wintertime) and warm period (for convenience, we call it summertime), we used the data of wintertime (April to October) and summertime
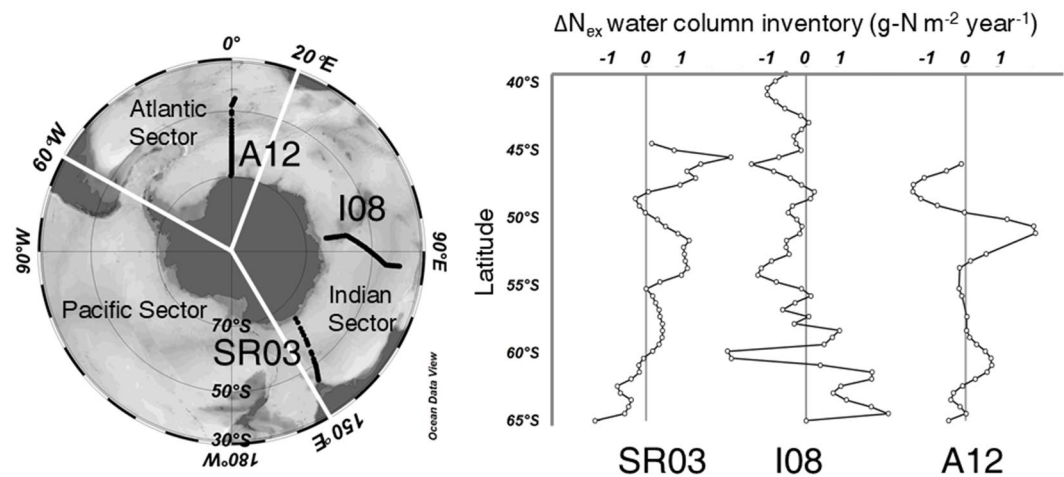
Figure 1. Meridional distributions of water column inventory of ΔN_{ex} along three lines in the SO. SR03 (left, from 1991 to 2011), I08 (middle, from 1994 to 2016), and A12 (right, from 1992 to 2014), as the annual rate of water column inventory of ΔN_{ex} during the period from the 1990s to the 2010s, in units of g-N m^{-2} year^{-1}. The inventories were determined by integrating from the surface to the sea floor. White lines separate the three sectors of the SO (the Pacific sector, the Indian sector, and the Atlantic sector). This figure was drawn using Ocean Data View[31].
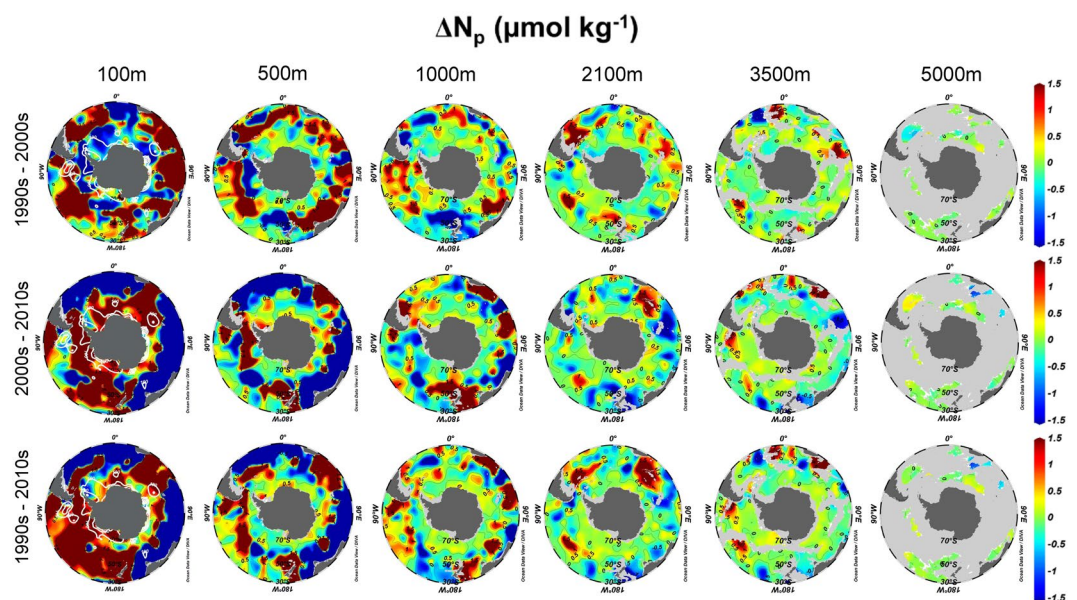
Figure 2. Horizontal distributions of the decadal change in N_p in the SO. Shown were ΔN_p from the 1990s to the 2000s (top row), 2000s to 2010s (middle row), and 1990s to 2010s (bottom row) at different depths, in units of μmol kg^{-1}. Grey areas show the sea floors. White contour lines indicate the regions where the mixed layer is deeper than 100 m. This figure was drawn using Ocean Data View[31].

(January to March) and calculated the average N_{obs} and N_p at each depth for these two durations (Fig. S8). We found that above the depth of 500 m the differences of both N_{obs} and N_p between the two seasons were ~3 μmol kg^{-1} as maximum; the corresponding differences at the depth of around 200 m became ~0.80 μmol kg^{-1}, which was equal to the RMSE of our parameterization. These two periods did not show an obvious difference below the depth of 500 m. Thus, we concluded that the seasonal difference in the observational data does not significantly affect the spatiotemporal distributions of ΔN_{ex} along with the total water column inventory.

The spatiotemporal distributions of ΔN_p and ΔN_{ex} are shown in Figs. 2 and 3(a), respectively. The spatiotemporal distribution of ΔN_p (Fig. 2) showed a large variation in the upper 1,000 m water column and it revolved around the Antarctic continent along with the Antarctic Circumpolar Current in the different time periods. This phenomenon may be due to the continuing enhanced nutrient-rich Circumpolar Deep Water upwelling derived from the strengthening of the Southern Hemisphere westerlies in recent decades[17,18]. Furthermore, ΔN_p became
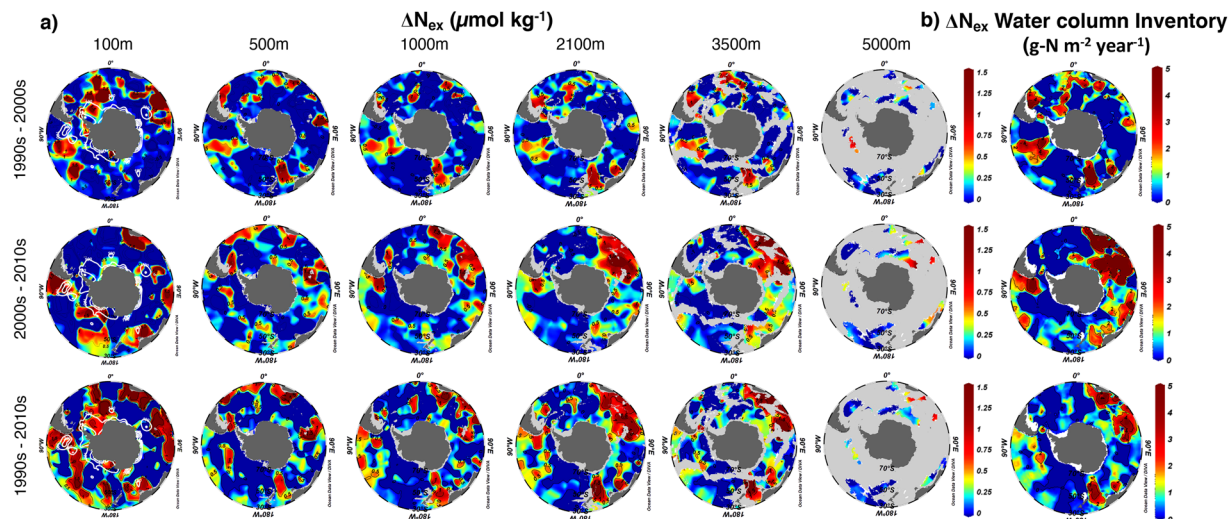
Figure 3. Horizontal distributions of the decadal change in N_{ex} in the SO. Shown along with the annual rate of change in the SO south of 30°S. (**a**) The decadal change in N_{ex} during the period from the 1990s to the 2000s (top row), 2000s to 2010s (middle row), and 1990s to 2010s (bottom row) at different depths. Scale was fixed from 0 to 1.5 µmol kg^{-1} to emphasize the increase in N_{ex}. Grey areas show the sea floors. (**b**) Total water column inventories of ΔN_{ex} as the annual rate of change in N_{ex} over the same periods as in (**a**), in units of g-N m^{-2} year^{-1}. Inventories were determined by integrating ΔN_{ex} from the surface to the depth of 5,900 m. White contour lines indicate the regions where the mixed layer is deeper than 100 m. This figure was drawn using Ocean Data View[31].

Period	Pacific Sector	Indian Sector	Atlantic Sector	Southern Ocean
1990s–2000s	25 ± 1	-4 ± 1	17 ± 1	38 ± 2
2000s–2010s	24 ± 1	100 ± 2	-22 ± 1	102 ± 3
1990s–2010s	24 ± 1	42 ± 1	0.02 ± 0	67 ± 1

Table 1. Total water column inventory of ΔN_{ex} in the SO. From the surface to 5,900-m depth south of 30°S during the 1990s – 2010s (Tg-N year^{-1}) (Pacific Sector: 150°E – 60°W; Indian Sector: 20°E – 150°E; Atlantic Sector: 60°W – 20°E). The uncertainty is the value of the standard error divided by the average of each sector (see Table S6 for detail).

zero gradually with the increase of depth, implying that there is almost no nature-derived variation of N in the deeper water column. The distribution of ΔN_p showed no obvious difference between the Pacific, the Indian and the Atlantic sector of the SO.

In Fig. 3(a), the spatial distribution of ΔN_{ex} in the surface layer shows a tendency to diffuse along the continental coastal area to the open ocean (e.g. west coast of South America, southwest coast of South Africa, and south of Tasmania, Australia). The data for the continental shelf were removed to eliminate the uncertainty of river input in our parameterization construction based on the assumption that the riverine N_{ex} has little effect on the open ocean[1] (see Supplementary Text S1). Jickells *et al.* (2017) found that approximately 75% of riverine N escapes beyond the shelf break and enters the open ocean, which may partly explain the significant rise in N_{ex} in the coastal region in our study[5].

In terms of the temporal distribution of ΔN_{ex}, the Indian sector has shown a remarkable growth in N_{ex} from the surface to the abyss during the period from the 2000s to the 2010s. By analyzing the spatiotemporal distribution, the reason for this can be attributed to the increase in anthropogenic nitrogen emission in developing countries such as India, China, and Southern Africa in the past decade[5,19,20]. According to the evaluation of the global meridional overturning circulation, the upwelling water in the surface North Pacific Ocean passes through the Strait of Malacca and reaches the northern Indian Ocean. Then, it goes south and flows into the Southern Ocean[7]. Meanwhile, the surface anthropogenic N is loaded on these waters along the coastal regions and brought to the Southern Ocean. Additionally, the enhancement of the Southern Annular Mode mentioned in the previous section can explain the increase in N_{ex} in the ocean interior.

We also estimated the total water column inventory of ΔN_{ex} from the surface to the sea floor in the SO (Fig. 3(b) and Table 1). During the 1990s to the 2010s, N_{ex} in the Pacific, Indian, and Atlantic sectors grew at the rate of 24 ± 1, 42 ± 1, and 0.02 ± 0 Tg-N year^{-1}, respectively, and that for the entire SO grew at the rate of 67 ± 1 Tg-N year^{-1}. Uncertainties were given by the standard error of gridding estimation (Table S6). The ΔN_{ex} in the Indian sector accounted for 63% of the increase in N_{ex} in the SO. We also found that the Atlantic Sector, which has the most active vertical circulation in the world, did not show a high ΔN_{ex}. This may be because of the following

two reasons: (1) the deviation caused by the seasonal differences in the surface data (Fig. S8); (2) the inflow of the deposition of N_{ex} from the Atlantic sector into the Indian sector due to the Antarctic Circumpolar Current, which also explains why ΔN_{ex} in the Indian sector is extremely high. In the Pacific Ocean, we mainly observed the accumulation of ΔN_{ex} in the surface layer (Fig. 3) due to the upwelling area with relatively old water age in the deep Pacific[21]. These results can be considered reasonable compared with the previous model predictions[1,5].

In an early study[1], the deposition rate of N_{ex} to the global ocean was predicted as 67 ± 30 Tg-N year^{-1} in the 2000s, the upper limit of which was 96 Tg-N year^{-1} considering the potential impact of riverine input. By comparing the deposition rate with our data, we found that the SO had received 69% of the global oceanic N_{ex} input despite the SO covering only 29% of the global ocean surface area, which emphasizes the important role of the SO in integrating anthropogenic impacts in the global ocean.

Conclusions

We presented the spatiotemporal distributions of ΔN_p and ΔN_{ex} in the SO from the 1990s to the 2010s using the simple parameterization of the predicted N along with the observed N ($R^2 = 0.97$; RMSE $= 0.80$ µmol kg^{-1}). In the Indian sector, which borders several developing countries, N_{ex} has grown at a rate of 42 ± 1 Tg-N year^{-1}, accounting for approximately 63% of the overall rate of increase of the SO (67 ± 1 Tg-N year^{-1}). y comparing our result with the global deposition rate reported by Duce *et al.*[1], the SO was found to receive approximately 70% of the global oceanic input of N_{ex} despite it covering only one-third of the global ocean area. In the future, a more detailed evaluation of N in the SO can be obtained by relying largely on ship-based observations and/or applying this parameterization method to autonomous biogeochemical Argo floats and CTD sensors[22–30].

References

1. Duce, R. A. *et al*. Impacts of Atmospheric Anthropogenic Nitrogen on the Open. *Ocean. Science* **320**, 893–897 (2008).
2. Gruber, N. & Galloway, J. N. An Earth-system perspective of the global nitrogen cycle. *Nature* **451**, 293–296 (2008).
3. Capone, D. G., Bronk, D. A., Mulholland, M. R. & Carpenter, E. J. *Nitrogen in the Marine Environment*. (Elsevier, 2008).
4. Gruber, N. The Dynamics of the Marine Nitrogen Cycle and its Influence on Atmospheric CO_2 Variations. in *The Ocean Carbon Cycle and Climate* 97–148 (Springer Netherlands), https://doi.org/10.1007/978-1-4020-2087-2_4 (2004).
5. Jickells, T. D. *et al*. A reevaluation of the magnitude and impacts of anthropogenic atmospheric nitrogen inputs on the ocean. *Global Biogeochem. Cycles* **31**, 289–305 (2017).
6. Kim, I. *et al*. Increasing anthropogenic nitrogen in the North Pacific. *Ocean. Science* **346**, 1102–1107 (2014).
7. Marshall, J. & Speer, K. Closure of the meridional overturning circulation through Southern Ocean upwelling. *Nat. Geosci.* **5**, 171–180 (2012).
8. Woosley, R. J., Millero, F. J. & Wanninkhof, R. Rapid anthropogenic changes in CO_2 and pH in the Atlantic Ocean: 2003–2014. *Global Biogeochem. Cycles* **30**, 70–90 (2016).
9. Panassa, E. *et al*. Variability of nutrients and carbon dioxide in the Antarctic Intermediate Water between 1990 and 2014. *Ocean Dyn.* **68**, 295–308 (2018).
10. Watanabe, Y. W., Li, B. F. & Wakita, M. Long-Term Trends of Direct and Indirect Anthropogenic Effects on Changes in Ocean pH. *Geophys. Res. Lett.* **45**, 9106–9113 (2018).
11. Li, B. F., Watanabe, Y. W. & Yamaguchi, A. Spatiotemporal distribution of seawater pH in the North Pacific subpolar region by using the parameterization technique. *J. Geophys. Res.* **121**, 3435–3449 (2016).
12. Lauvset, S. K. *et al*. A new global interior ocean mapped climatology: The 1° × 1° GLODAP version 2. *Earth Syst. Sci. Data* **8**, 325–340 (2016).
13. Olsen, A. *et al*. The global ocean data analysis project version 2 (GLODAPv2) - An internally consistent data product for the world ocean. *Earth Syst. Sci. Data* **8**, 297–323 (2016).
14. Gregg, W. W., Conkright, M. E., Ginoux, P., O'Reilly, J. E. & Casey, N. W. Ocean primary production and climate: Global decadal changes. *Geophys. Res. Lett.* **30** (2003).
15. Carter, L., McCave, I. N. & Williams, M. J. M. Chapter 4 Circulation and Water Masses of the Southern Ocean: A Review. *Dev. Earth Environ. Sci* **8**, 85–114 (2008).
16. Thompson, D. W. J. *et al*. Signatures of the Antarctic ozone hole in Southern Hemisphere surface climate change. *Nat. Geosci.* **4**, 741–749 (2011).
17. Menviel, L. *et al*. Southern Hemisphere westerlies as a driver of the early deglacial atmospheric CO2 rise. *Nat. Commun.* **9**, 1–12 (2018).
18. Peck, V. L., Allen, C. S., Kender, S., McClymont, E. L. & Hodgson, D. Oceanographic variability on the West Antarctic Peninsula during the Holocene and the influence of upper circumpolar deep water. *Quat. Sci. Rev.* **119**, 54–65 (2015).
19. Liu, X. *et al*. Enhanced nitrogen deposition over China. *Nature* **494**, 459–462 (2013).
20. Oita, A. *et al*. Substantial nitrogen pollution embedded in international trade. *Nat. Geosci.* **9**, 111–115 (2016).
21. Sarmiento, J. L. & Gruber, N. *Ocean Biogeochemical Dynamics*. (Princeton University Press, New Jersey, 2006).
22. Olsen, A. *et al*. GLODAPv2.2019 – an update of GLODAPv2. *Earth Syst. Sci. Data Discuss.* 1–39, https://doi.org/10.5194/essd-2019-66 (2019).
23. de Boyer Montegut, C., Madec, G., Fischer, A. S., Lazar, A. & Iudicone, D. Mixed layer depth over the global ocean: An examination of profile data and a profile-based climatology. *J. Geophys. Res.* **109** (2004).
24. Emery, W. J. Water Types and Water Masses. in *Ocean circulation/Water Types and Water Masses* 1556–1567 (University of Colorado, Boulder), https://doi.org/10.1016/b0-12-227090-8/00279-7 (2003).
25. Wilks, D. S. *Statistical methods in the atmospheric sciences*. (Academic Press,N.Y., 2011).
26. Switzer, A. C. Mapping nitrate in the global ocean using remotely sensed sea surface temperature. *J. Geophys. Res.* **108** (2003).
27. Orsi, Alejandro H. Whitworth & Thomas, I. *WOCE Southern Ocean.* **1** (2005).
28. Ishizu, M. & Richards, K. J. Relationship between oxygen, nitrate, and phosphate in the world ocean based on potential temperature. *J. Geophys. Res.* **118**, 3586–3594 (2013).
29. Anderson, L. A. & Sarmiento, J. L. Redfield ratios of remineralization determined by nutrient data analysis. *Global Biogeochem. Cycles* **8**, 65–80 (1994).
30. Stramma, L., Schmidtko, S., Levin, L. A. & Johnson, G. C. Ocean oxygen minima expansions and their biological impacts. *Deep. Res. Part I Oceanogr. Res. Pap* **57**, 587–595 (2010).
31. Schkizer, R. https://odv.awi.de, (2020).

Author contributions

X.L.P. and Y.W.W. provided the first idea of this paper; X.L.P. collected the data; X.L.P. and B.F.L. analyzed the data; X.L.P., B.F.L. and Y.W.W. co-wrote the paper.

Competing interests

The authors declare no competing interests.

Additional information

Supplementary information is available for this paper at https://doi.org/10.1038/s41598-020-65661-2.

Correspondence and requests for materials should be addressed to X.L.P.

Reprints and permissions information is available at www.nature.com/reprints.

Publisher's note Springer Nature remains neutral with regard to jurisdictional claims in published maps and institutional affiliations.